


NANO EXPRESS

Open Access

Flexible Transparent Electrodes Based on Gold Nanomeshes



Zeping Li^{1*} , Geng Wang¹, Zhongming Li¹, Zhengze Cheng¹, Guopeng Zhou¹ and Shan Li²

Abstract

The transmittance, conductivity, and flexibility are the crucial properties for the development of next-generation flexible electrodes. Achieving a good trade-off between transmittance and conductivity of flexible electrodes has been a challenge because the two properties are inversely proportional. Herein, we reveal a good trade-off between transmittance and conductivity of gold nanomesh (AuNM) can be achieved through appropriately increasing the AuNM thickness no more than 40 nm, the mean free path of electrons in Au metal. The further flexibility investigation indicates that the AuNM electrodes with mesh structure show higher tolerance than the Au bulk film, and the AuNM electrodes with smaller inter-aperture wire width can accommodate more tensile strains than a counterpart with bigger inter-aperture wire width. The simulated results based on finite element analysis (FEA) show good agreement with experimental results, which indicates the fabrication method of versatile nanosphere lithography (NSL) is reliable. These results established a promising approach toward next-generation large-scale flexible transparent AuNM electrodes for flexible electronics.

Keywords: AuNM, NSL, FEA, Transmittance, Sheet resistance, Flexibility

Introduction

Recently, novel flexible transparent electrodes have been investigated, such as doped metal oxides (ITO, FTO), carbon nanotubes, graphene, and conducting polymers, to enable electrical conductivity and optical transparency simultaneously under mechanical deformation. [1–5]. ITO and FTO suffer from manufacturing cost and brittleness due to their ceramic nature, which confines the application on irregular surfaces [6, 7]. The poor environmental stability and biocompatibility of conducting polymers by reason of the instability of the doped state have been unresolved [8]. One primary strategy is to use highly conductive metal nanomesh materials on an elastic substrate [9]. The metal film as transparent electrodes stems largely from their typically high free-electron density, which enables ultrathin metal film on the order of 1–40 nm thickness to have optical transparency and appropriate conductivity [10]. However, a single ultrathin metal film cannot have high transmittance because of the high surface reflection even if absorption inside the metal film

is negligible by setting its thickness comparable to the skin depth [11, 12]. To address the issues, the nanostructured transparent metal electrodes have been recently developed to allow the light to pass through and conceivably achieve high optical transmission while maintaining the low sheet resistance of the metal and effective flexibility [13–17]. Silver nanowire showed low sheet resistance and high transparency as flexible transparent electrodes for replacing ITO [13–15]. However, several drawbacks, such as large junction resistance, small contact area, and easy corrosion due to oxidation and sulfur vulcanization, degraded the performance of the silver nanowire electrodes [10]. Considering the issue of long-term stability, some metals such as Au and Pt should be developed firstly, by virtue of their long-term electrical stability without corroding through oxidation [16, 17]. The transparent AuNM electrodes with mesh-like topology have been increasingly explored for better performance [18, 19]. However, achieving a good trade-off between transmittance and conductivity of AuNM has been a challenge because the two properties are inversely proportional [20, 21]. The influence of mesh size on mechanical flexibility properties has not been investigated for them to be applied to flexible electronics [22].

* Correspondence: D201477516@alumni.hust.edu.cn

¹School of Electronic Information and Engineering, Hubei University of Science and Technology, Xianning 437005, Hubei, People's Republic of China
Full list of author information is available at the end of the article

In this paper, we demonstrate the flexible transparent AuNM electrodes made by the versatile nanosphere lithography (NSL) technique [23–25]. The resulting AuNM electrode with hexagonal, uniform, and periodic nanostructure exhibited excellent transmittance and sheet resistance. The simulated results based on finite element analysis (FEA) show good agreement with experimental results, and the results reveal a good trade-off between transmittance and conductivity of AuNM can be achieved through appropriately increasing the AuNM thickness no more than 40 nm. The further flexibility investigation indicates that the AuNM electrodes with mesh structure show higher tolerance than the Au bulk film, and the AuNM electrodes with smaller inter-aperture wire width can accommodate more tensile strains than a counterpart with bigger inter-aperture wire width. The bench tests indicate the prepared AuNM electrodes possess high transmittance, low sheet resistance, and excellent flexibility.

Methods and Experiments

Experimental Details

NSL attracts more and more attention as an inexpensive and wafer-scale technique for the fabrication of ordered, uniform, and tunable nanostructure utilizing a hexagonally close-packed monolayer of polystyrene spheres (PS, Aladdin Co., Ltd.) as a template [26–28].

Figure 1a shows the fabrication process for AuNM using the NSL technique. (i) After a close-packed monolayer of PS spheres with an initial diameter $D = 1 \mu\text{m}$ was deposited onto a 500- μm -thick polyethylene terephthalate (PET, Aladdin Co., Ltd.) substrate on glass, which was cleaned with isopropanol and deionized water sequentially via an air/water interface with self-assembly, the diameter of the PS spheres was reduced via reactive ion etching (RIE, etching gases: O_2 and CHF_3) to create gaps between the PS spheres. (ii) Metal nanomesh was

formed in the vacancies between the PS spheres after the deposition of 2 nm Ti buffer layer and 20 nm Au via electron beam evaporation. (iii) After PS spheres were removed by an adhesive tape and sonication, the metal nanomesh on substrate was yielded. The obtained microstructures were characterized by a scanning electron microscope (SEM, Nova NanoSEM 450, FEI, Eindhoven, Netherlands). To visually demonstrate the performance of transmittance and sheet resistance under strain tension, we developed a measurement setup as shown in Fig. 1b. In this test, a typical AuNM membrane with $\sim 160 \text{ nm}$ average inter-aperture wire width and $\sim 20 \text{ nm}$ thickness on PET film (thickness $\sim 500 \mu\text{m}$) was adopted. The transparent and bent AuNM electrode under strain tension is connected with the wire by conductive silver paste and conductive copper tape for good electrical contact, yielding lit of LED, as shown in Fig. 1b. This test indicates the prepared AuNM electrodes possess high transmittance, low sheet resistance, and excellent flexibility.

As shown in Fig. 2a, the prepared AuNM has a precisely controlled nanostructure showing excellent uniformity with hexagonally arrayed periodic circular holes. The six different AuNM samples with averaged inter-aperture wire width, namely the vacancies between two PS spheres (labeled as “w,” varying from 100 nm to 175 nm, $w_1 = 100 \text{ nm}$, $w_2 = 115 \text{ nm}$, $w_3 = 130 \text{ nm}$, $w_4 = 145 \text{ nm}$, $w_5 = 160 \text{ nm}$, $w_6 = 175 \text{ nm}$), were prepared for comparison.

Simulation Details

For comparison, the six different numerical models (Fig. 2b) with the same parameters as the prepared AuNM samples have been analyzed in the FEA simulation.

In the electromagnetic simulations, the light source was set to create circularly polarized light on a unit cell of AuNM on PET, as shown in Additional file 1: Figure

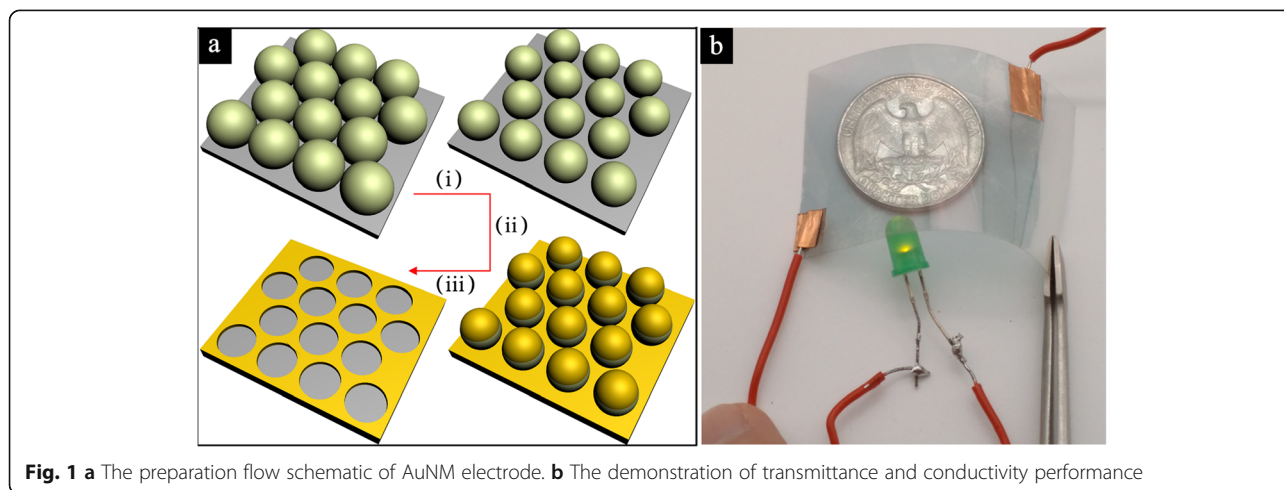


Fig. 1 a The preparation flow schematic of AuNM electrode. b The demonstration of transmittance and conductivity performance

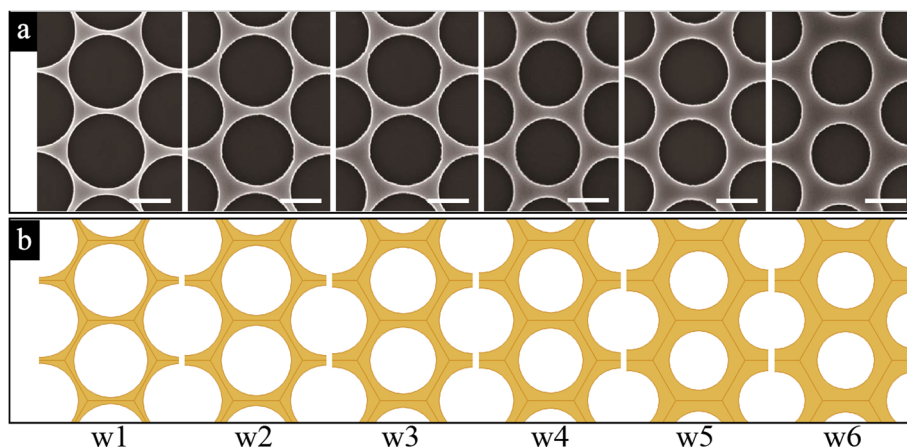


Fig. 2 The structure images of AuNM. **a** Top-view SEM images of six different experimental samples, and **b** top-view drawings of six different numerical models. Scale bar: 500 nm

S1. An integrating sphere was used to measure the total transmitted light and not simply the specular transmittance. Periodic boundary conditions were used to simulate in one unit cell at the horizontal directions. And perfectly matched layer boundary conditions were used to prevent unphysical scattering at the edge of the simulated unit cell in the vertical directions [29]. Further, parameters of material properties were applied from the published experimental data, which were the same for the material of mechanic simulations [30]. Additional file 1: Figure S2 shows a schematic diagram of the models of AuNM and AuNM on PET in mechanical flexibility simulation, respectively.

Results and Discussions

The theoretical model is validated by comparing the simulated results with the experimental data. The transmittance at 550 nm and sheet resistance properties of six different samples based on the simulated and experimental data are demonstrated in Fig. 3. Along with the increase of inter-aperture wire width, both of the transmittance and the sheet resistance decreased. In particular, the variation trend of simulated data is linear. The measured transmittance and sheet resistance properties are in agreement with the simulated properties, which indicate the NSL fabrication method is reliable. The largest transmittance of 89% and sheet resistance of

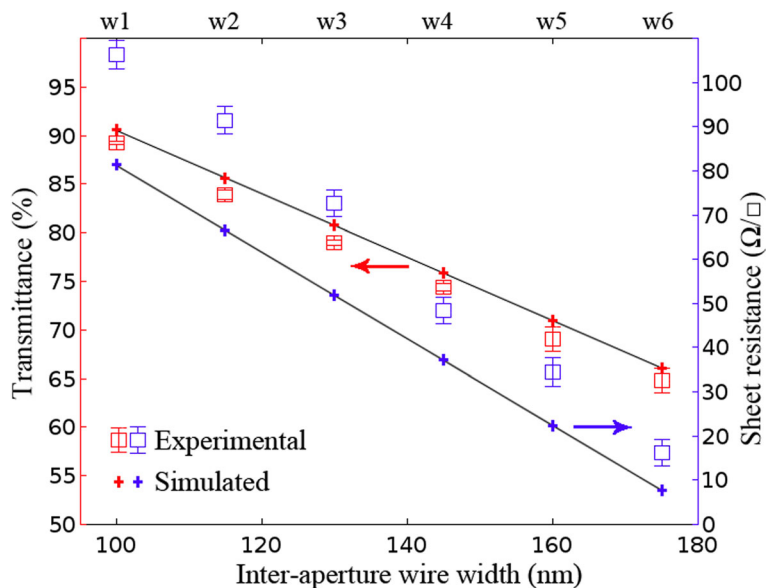


Fig. 3 Transmittance and sheet resistance vs. inter-aperture wire width of AuNM (at $\lambda = 550$ nm and thickness = 20 nm)

104.5 Ω/\square were measured at the smallest wire width of 100 nm, and the largest wire width of 175 nm yields transmittance of 65% and sheet resistance of 16.5 Ω/\square . From geometric considerations, higher transmittance derives from bigger apertures, namely smaller wire width due to the decrease of etching time for PS spheres, which results in a decreased area to block the light. However, smaller wire width results in increasing the sheet resistance due to decreased conducting pathways for electrons to flow.

It should be noted that the transmittance and sheet resistance decreased linearly as the inter-aperture wire width increased in simulated results is by virtue of perfect periodicity of simulated models. On the contrary, performances of transmittance and sheet resistance in the experimental results suffer from degradation due to more or less some inevitable defects, impurities, and surface roughness.

In order to maximize the potential of AuNM for use as a transparent electrode, it is typically desirable to have a high transmission and a low sheet resistance. However, achieving a good trade-off between transmittance and conductivity of AuNM has been a challenge because the two properties are inversely proportional. To address the issue, herein, we analyzed theoretically the effect of AuNM thickness on transmittance and sheet resistance. All the simulations were performed at the same 550 nm wavelength, 160 nm averaged inter-aperture wire width, and 10 to 100 nm thickness. Additional file 1: Figure S3 shows the potential distribution map of AuNM at constant current. At the initial stage in Fig. 4, the increase of AuNM thickness results in a rapid decrease of sheet resistance, which decreases slowly after the thickness of 40 nm. The thicker AuNM beyond 40 nm close to the

mean free path of electrons in Au metal cannot significantly increase the conductivity [31]. Meanwhile, high transmittance has been maintained for a long time, which decreases slowly. Thicker AuNM would increase conducting pathways for electrons to flow, which yields a low sheet resistance with a slight degradation of transmission due to constant apertures and wire width.

Efforts could be dedicated to improve the transmittance and conductivity of such metal nanomesh by appropriately increasing the AuNM thickness no more than 40 nm, the mean free path of electrons in Au metal.

One compelling property of AuNM is good mechanical flexibility. The influence of strain on the sheet resistance was investigated to examine the mechanical flexibility of the AuNM under bending. In order to facilitate analysis, a sample of Au bulk film with the same parameters as a model counterpart of numerical Au bulk film (thickness ~ 20 nm) on PET film (thickness ~ 500 μm) has been fabricated. The insets show maps of the AuNM electrodes during bending test and bending simulation, respectively. Additional file 1: Figure S4 shows the stress distribution map of the AuNM electrodes during bending simulation under 1.5×10^9 N/m² force at the Y direction, which shows that stress is mainly concentrated in the center of AuNM. As shown as Fig. 5, in the bending test, firstly, the Au bulk film with maximum inter-aperture wire width exhibited a dramatic increase of the sheet resistance at strain beyond 1.9 % and the worst flexible performance. However, six AuNM electrodes remained their initial resistance until the stretch ratio reaches 2.1 %. At the same time, as inter-aperture wire widths decreased, the AuNM electrodes suffer from electrical failure gradually, due to the breakdown of the AuNM electrodes entirely.

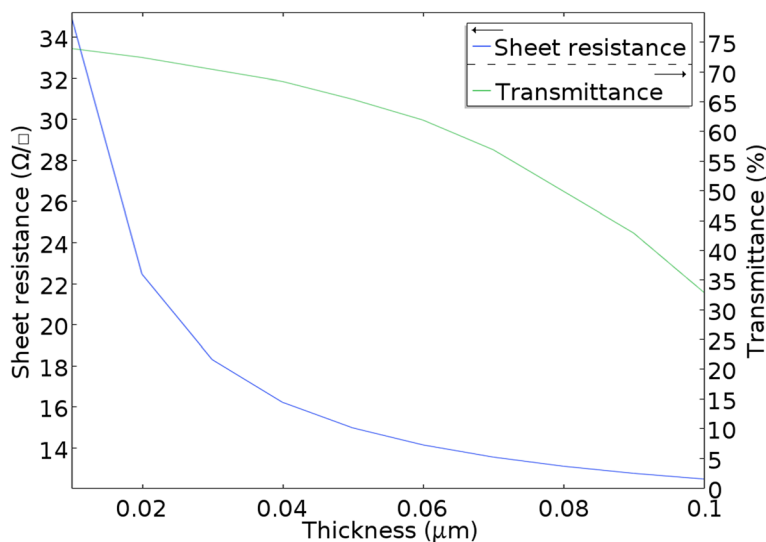
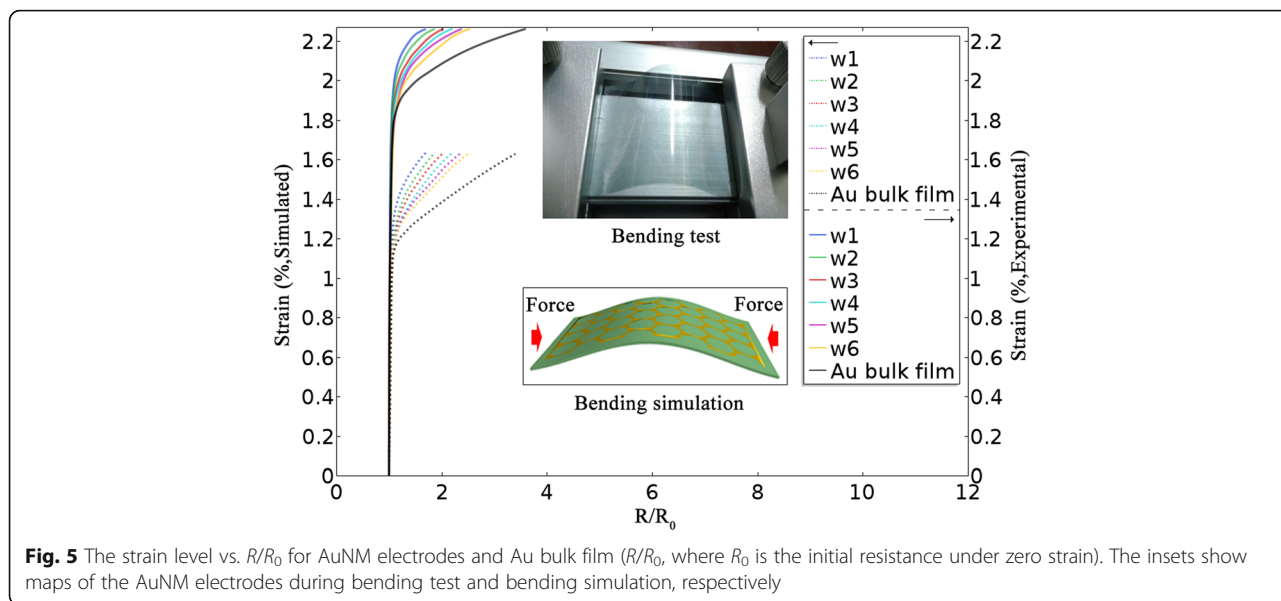


Fig. 4 Transmittance and sheet resistance vs. the AuNM thickness (at $\lambda = 550$ nm and $W_5 = 160$ nm)



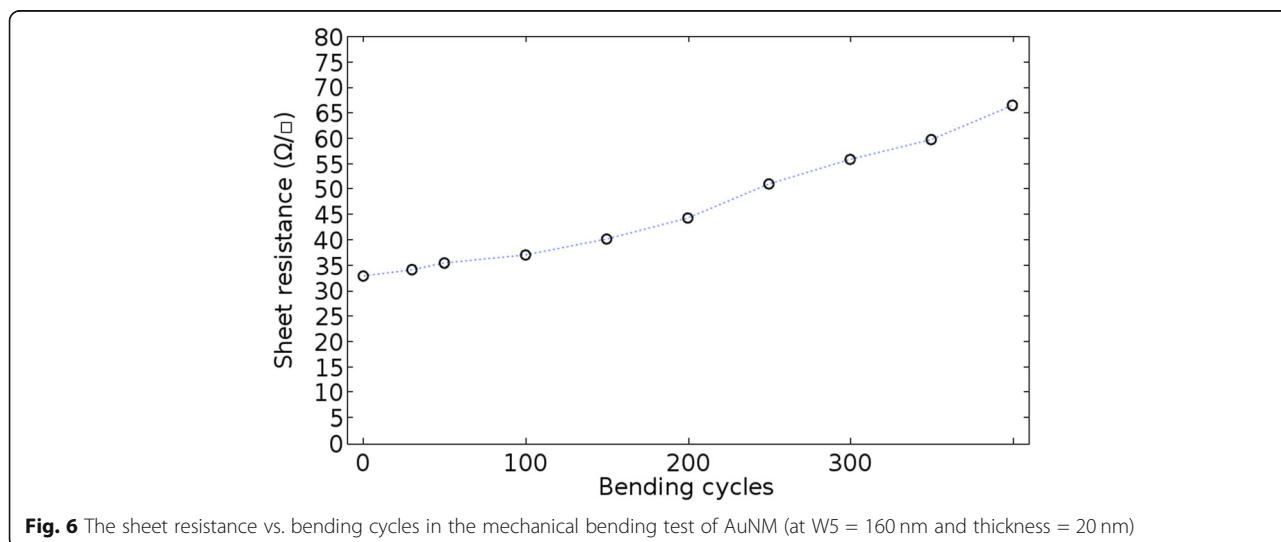
It is not hard to find the AuNM electrodes with a mesh structure showing higher tolerance than the Au bulk film, and the AuNM electrodes with smaller inter-aperture wire width exhibit better flexible performance. The applied force on samples will cause tensile strain, which can be accommodated by in-plane rotations and distortion of periodic nanomesh without breakage of AuNM [32]. However, Au bulk film cannot accommodate the applied tensile strains, which cause its breakage at the threshold point of tensile strains and electrical failure.

The simulated results show good agreement with experimental results except that the threshold point of tensile strains in the simulated results (closed to 1.2) is lower than the experimental results. This is due to the fabricated samples with a size of several

square centimeters can accommodate more tensile strains than the simulated models with a size of several square microns.

In addition, to assess the electrode stability, the sheet resistance value of the AuNM electrodes was measured as bending test progressed. AuNM electrodes on PET film were bent up to 400 cycles under a minimum radius of curvature of 5 mm and maximum of 15 mm, as shown in Fig. 6, showing the good flexible stability.

Conclusions In conclusion, the present results show the flexible transparent AuNM electrodes can be synthesized using the versatile NSL technique. The resulting AuNM electrode with hexagonal, uniform, and periodic nanostructure exhibited excellent transmittance and sheet resistance. The simulated results show good agreement



with experimental results, which indicate the NSL fabrication method is reliable. A good trade-off between transmittance and conductivity of AuNM can be achieved through appropriately increasing the AuNM thickness no more than 40 nm, the mean free path of electrons in Au metal. In the flexibility investigation, the AuNM electrodes with mesh structure show higher tolerance than the Au bulk film, and the AuNM electrodes with smaller inter-aperture wire width can accommodate more tensile strains than a counterpart with bigger inter-aperture wire width; the mechanical bending test shows the good flexible stability of AuNM. The prepared AuNM electrodes with high transmittance, low sheet resistance, and excellent flexibility established a promising approach toward next-generation large-scale flexible transparent AuNM electrodes, with broad utility for applications in flexible electronics including biosensors and optoelectronic devices.

Additional file

Additional file 1: Figure S1. Schematic diagram of the simulated unit cell of AuNM on PET. (a) Top view. (b) Perspective view. **Figure S2.** Schematic diagram of the simulated models. (a) AuNM. (b) AuNM on PET. **Figure S3.** The potential distribution map of AuNM at constant current. **Figure S4.** The stress distribution map of the AuNM electrodes during bending simulation under $1.5 \times 10^9 \text{ N/m}^2$ force at the Y direction. (DOC 1287 kb)

Abbreviations

AuNM: Gold nanomesh; FEA: Finite element analysis; NSL: Nanosphere lithography; PET: Polyethylene terephthalate; PS: Polystyrene spheres; SEM: Scanning electron microscope

Acknowledgements

The authors acknowledge the financial support given for this work by the Scientific Research Project of Education Department of Hubei Province under B2017174 and B2017172.

Funding

This work is supported by the Scientific Research Project of Education Department of Hubei Province (Grant Nos. B2017174 and B2017172).

Availability of Data and Materials

Data available on request from the authors

Authors' Contributions

ZPL and GW designed the experiments. ZPL performed the experiments and the simulation. ZPL drafted the manuscript. Other authors contributed to the data analysis and manuscript modification. All authors read and approved the final manuscript.

Competing Interests

The authors declare that they have no competing interests.

Publisher's Note

Springer Nature remains neutral with regard to jurisdictional claims in published maps and institutional affiliations.

Author details

¹School of Electronic Information and Engineering, Hubei University of Science and Technology, Xianning 437005, Hubei, People's Republic of China. ²School of Petrochemical Engineering, Changzhou University, Changzhou 213164, Jiangsu, People's Republic of China.

Received: 27 December 2018 Accepted: 3 April 2019

Published online: 16 April 2019

References

- Wang X, Shen G (2015) Intercalation pseudo-capacitive TiNb_2O_7 @carbon electrode for high-performance lithium ion hybrid electrochemical supercapacitors with ultrahigh energy density. *Nano Energy* 15:104–115
- Cui F, Yu Y, Dou L, Sun J, Yang Q, Schildknecht C et al (2015) Synthesis of ultrathin copper nanowires using tris(trimethylsilyl)silane for high-performance and low-haze transparent conductors. *Nano Lett* 15:7610–7615
- Schneider J, Rohner P, Thureja D, Schmid M, Galliker P, Poulikakos D (2015) Electrohydrodynamic nanodrip printing of high aspect ratio metal grid transparent electrodes. *Adv Funct Mater* 26(6):833–840
- Li L, Lou Z, Han W, Chen D, Jiang K, Shen G (2017) Highly stretchable micro-supercapacitor arrays with hybrid MWCNT/PANI electrodes. *Adv Mater Technol* 2(3):1600282
- Chung WH, Park SH, Joo SJ, Kim HS (2018) UV-assisted flash light welding process to fabricate silver nanowire/graphene on a PET substrate for transparent electrodes. *Nano Res* 11:2190–2203
- Jang YR, Chung WH, Hwang YT, Kim SH, Kim HS (2018) Selective wavelength plasmonic flash light welding of silver nanowires for transparent electrodes with high conductivity. *ACS Appl Mater Interfaces* 10:24099–24107
- Maurer JHM, González-García L, Reiser B, Kanelidis I, Kraus T (2016) Templated self-assembly of ultrathin gold nanowires by nanoimprinting for transparent flexible electronics. *Nano Lett* 16:2921–2925
- Kaur G, Adhikari R, Cass P, Bown M, Gunatillake P (2015) Electrically conductive polymers and composites for biomedical applications. *RSC Adv* 5:37553–37567
- Won Y, Kim A, Yang W, Jeong S, Moon J (2014) A highly stretchable, helical copper nanowire conductor exhibiting a stretchability of 700%. *NPG Asia Mater* 6:132
- Ghosh DS (2013) Ultrathin metal transparent electrodes for the optoelectronics industry. Springer Theses Springer, Berlin
- Wang S, Wang ZL, Yang Y (2016) A one-structure-based hybridized nanogenerator for scavenging mechanical and thermal energies by triboelectric-piezoelectric-pyroelectric effects. *Adv Mater* 28:2881–2887
- Han B, Peng Q, Li R, Rong Q, Ding Y, Akinoglu EM et al (2016) Optimization of hierarchical structure and nanoscale-enabled plasmonic refraction for window electrodes in photovoltaics. *Nat Commun* 7:12825
- Mou Y, Cheng H, Wang H, Sun Q, Liu J, Peng Y et al (2019) Facile preparation of stable reactive silver ink for highly conductive and flexible electrodes. *Appl Surf Sci* 475:75–82
- Mou Y, Zhang Y, Cheng H, Peng Y, Chen M (2018) Fabrication of highly conductive and flexible printed electronics by low temperature sintering reactive silver ink. *Appl Surf Sci* 459:249–256
- Kang H, Song SJ, Sul YE, An BS, Yin Z, Choi Y et al (2018) Epitaxial-growth-induced junction welding of silver nanowire network electrodes. *ACS Nano* 12(5):4894–4902
- Sun M, Zhang F, Tong ZH, Sheng GP, Chen YZ, Zhao Y et al (2010) A gold-sputtered carbon paper as an anode for improved electricity generation from a microbial fuel cell inoculated with *Shewanella oneidensis* MR-1. *Biosens Bioelectron* 26:338–343
- Ye S, Rathmell AR, Chen Z, Stewart IE, Wiley BJ (2014) Metal nanowire networks: the next generation of transparent conductors. *Adv Mater* 26(39):6670–6687
- Qiang Y, Seo KJ, Zhao XY, Artoni P, Golshan NH, Culaclii S et al (2017) Bilayer nanomesh structures for transparent recording and stimulating microelectrodes. *Adv Funct Mater* 27:1704117
- Khan Y, Pavinatto FJ, Lin MC, Liao A, Swisher SL, Mann K et al (2015) Inkjet-printed flexible gold electrode arrays for bioelectronic interfaces. *Adv Funct Mater* 26(7):1004–1013
- Qiu HJ, Guan YX, Luo P, Wang Y (2017) Recent advance in fabricating monolithic 3D porous graphene and their applications in biosensing and biofuel cells. *Biosens Bioelectron* 89:85–95
- Sanders M, Lin YB, Wei JJ et al (2014) An enhanced LSPR fiber-optic nanoprobe for ultrasensitive detection of protein biomarkers. *Biosens Bioelectron* 61:95–101
- Trung TQ, Lee N (2017) Materials and devices for transparent stretchable electronics. *J Mater Chem C* 5:2202

23. Haynes CL, Van Duyne RP (2001) Nanosphere lithography: a versatile nanofabrication tool for studies of size-dependent nanoparticle optics. *J Phys Chem B* 105:5599–5611
24. Zhang XY, Whitney AV, Zhao J, Hick EM, Van Duyne RP (2006) Advances in contemporary nanosphere lithographic techniques. *J Nanosci Nanotechnol* 6:1920–1934
25. Frey W, Woods CK, Chilkoti A (2000) Ultraflat nanosphere lithography: a new method to fabricate flat nanostructures. *Adv Mater* 12:1515
26. Plettl A, Enderle F, Saitner M, Manzke A, Pfahler C, Wiedemann S et al (2009) Non-close-packed crystals from self-assembled polystyrene spheres by isotropic plasma etching: adding flexibility to colloid lithography. *Adv Funct Mater* 19:3279–3284
27. Yan J, Yang LP, Lin MF, Ma J, Lu X, Lee PS (2013) Polydopamine spheres as active templates for convenient synthesis of various nanostructures. *Small* 9:596–603
28. Huang Z, Fang H, Zhu J (2007) Fabrication of silicon nanowire arrays with controlled diameter, length, and density. *Adv Mater* 19:744–748
29. Simicevic N, Haynie DT (2005) FDTD simulation of exposure of biological material to electromagnetic nanopulses. *Phys Med Biol* 50:347
30. Vayron R, Nguyen VH, Bos R (2015) Finite element simulation of ultrasonic wave propagation in a dental implant for biomechanical stability assessment. *Biomech Model Mechan* 14:1021–1032
31. Sondheimer EH (1952) The mean free path of electrons in metals. *Adv Phys* 1:1–42
32. Jang HY, Lee SK, Cho SH, Ahn JH, Park S (2013) Fabrication of metallic nanomesh: Pt nano-mesh as a proof of concept for stretchable and transparent electrodes. *Chem Mater* 25(17):3535–3538

Submit your manuscript to a SpringerOpen[®] journal and benefit from:

- ▶ Convenient online submission
- ▶ Rigorous peer review
- ▶ Open access: articles freely available online
- ▶ High visibility within the field
- ▶ Retaining the copyright to your article

Submit your next manuscript at ▶ [springeropen.com](https://www.springeropen.com)
